
Tomographic Reconstruction and Regularisation with Search Space Expansion and Total Variation

Mohammad Majid al-Rifaie* Tim Blackwell

School of Computing & Mathematical Sciences, University of Greenwich, London, UK

m.alrifaie@gre.ac.uk

Department of Computing, Goldsmiths College, University of London, London UK

t.blackwell@gold.ac.uk

Abstract

The use of ray projections to reconstruct images is a common technique in medical imaging. Dealing with incomplete data is particularly important when a patient is vulnerable to potentially damaging radiation or is unable to cope with the long scanning time. This paper utilises the reformulation of the problem into an optimisation tasks, followed by using a swarm-based reconstruction from highly undersampled data where particles move in image space in an attempt to minimise the reconstruction error. The process is prone to noise and, in addition to the recently introduced search space expansion technique, a further smoothing process, total variation regularisation, is adapted and investigated. The proposed method is shown to produce lower reproduction errors compared to standard tomographic reconstruction toolbox algorithms as well as one of the leading high-dimensional optimisers on the clinically important Shepp-Logan phantom.

1 Introduction

Tomographic reconstruction (TR), which is the determination of the internal structure of an opaque object from projected images cast by penetrating radiation, is at the heart of all medical imaging procedures (X-Ray CT, PET, MRI, Nuclear Medicine and ultrasound [24]) and has widespread application in various scientific fields, mathematics and industry [27, 36, 18, 13, 19, 25, 32, 16, 22].

As part of the imaging process, a number of projections is acquired which are often insufficient for a unique reconstruction. Given the under-determined nature of the problem, and the random nature of the radiation, the operating characteristics of the detectors and, in medical applications, patient movement, projection data is incomplete and noisy. The use of an accurate and fast image reconstruction algorithms with the ability to identify structures from reduced patient radiation dose (by weakening the incident radiation and/or reducing acquisition time) is a significant challenge. Success in this ‘few-view’ scenario would enable procedures that were once prohibited.

There are several reconstruction methods which address various challenges posed in the imaging procedure. Filtered backprojection (FBP), is a standard reconstruction technique, which operates with only a single iteration but is not suitable for few-view imaging [24]. With increased computational power, Algebraic Reconstruction Techniques (ART) have recently been in more common use. This class of methods are iterative algorithms based on Kaczmarz’s method [36] and, while capable of dealing with few-view scenarios, the added artefacts caused by overfitting is a known weakness. Furthermore, evidence of their worth in large patient populations is lacking [23].

*Corresponding author.

If the data is transformed to a sparse and therefore compressible representation, exact image reconstruction is feasible. Compressed Sensing (CS), which exploits this principle, shows promise for few-view reconstruction, but is heavily dependant on knowledge of the sparse representation, and on replacing the non-convex optimisation problem typically unsolvable by traditional methods, by a solvable convex minimisation [17].

Maximum-likelihood expectation maximisation (MLEM) and the more computationally efficient ordered subset expectation maximisation (OSEM) are iterative statistical methods which have been trialled and found to be superior to FBP in some cases e.g. [44, 39].

Reconstruction problems can be cast as optimisation tasks which opens up the possibility of using population based methods and other metaheuristics (e.g. [34, 28, 21, 12, 29, 40, 45, 26]). An ant algorithm has been developed for binary reconstruction [5]. TR problems and particularly, few-view tomography, is underdetermined: there are many solutions with zero reconstruction error but only some of these are medically feasible and representative of the original object. Artefacts and noise typically reduce reconstruction quality. The challenge is therefore to find biologically plausible solutions of low reconstruction error.

The research in this paper builds on the findings of reference [7] which introduced swarm optimisation with search space expansion (SSE). The idea behind SSE is a successive widening of the effective search space; clamping at each search space boundary favours homogeneity and significantly reduces noise. This work introduces a regularisation procedure in order to further smooth swarm reconstructions. A penalty term, proportional to image gradient, is added to the reconstruction error with the effect that the optimiser must minimise both reconstruction quality and pixel heterogeneity. This approach, known as Total Variation regularisation (TV), has previously been shown to aid CT reconstructions with traditional algorithms [38].

This paper compares the performance of FBP and ART toolbox reconstruction algorithms, and a gradient descent reconstruction procedure, CGLS, to a number of population based methods (local and global particle swarm optimisation (PSO), dispersive flies optimisation (DFO) and differential evolution (DE)). The best performing method is then subject to TR-optimised manifestations of SSE and TV. The results are further compared to a state-of-the art high-dimensional optimiser. The statistical analysis and the demonstrable visual reconstruction demonstrates the ability of the proposed method to reconstruct medically pertinent images from limited views.

2 Tomography and reconstruction

The problem in discrete reconstruction is:

$$\begin{aligned} \text{find } x &\in \{0, 1, \dots, k-1\}^n, k > 1 \\ \text{such that } Ax &= b \end{aligned} \quad (1)$$

where $b \in \mathbb{R}^m$ is the vector of detector values. A projection matrix, $A \in \mathbb{R}_{\geq 0}^{m \times n}$, where m is the total number of projections, and n is the number of pixels in the reconstructed image. We consider the problem as greyscale, where x is a vector of reconstructed pixel values and $k = 256$ i.e. $x \in \{0, 1 \dots, 255\}^n$.

The original object or the ground truth, denoted x^* , also satisfying $Ax^* = b$, is either a phantom (artificial test case) or an imaged subject. Given the under-deterministic nature of the problem, the equation $Ax = b$ cannot be inverted (few view, $m \ll n$) and there are multiple solutions. Suppose y is a trial solution; y is forward projected, and a *reconstruction* error, e_1 , evaluated,

$$e_1(y) = \|b - Ay\|_2^2. \quad (2)$$

Low reconstruction error does not imply faithfulness to the original object x^* . The distance between y to x^* can be measured by a *reproduction* error, e_2 , in instances where x^* is known:

$$e_2 = \|y - x^*\|_1 \quad (3)$$

The reproduction error provides a test of the algorithmic ability to find a feasible reconstruction.

Libraries such as the Astra toolbox [43] provide the forward projection operator A in addition to the standard reconstruction algorithms such as ART, FPB and SIRT. In the absence of real-world data,

and for algorithm development and comparison, a virtual phantom x^* is designed and $b = Ax^*$ is computed by forward projection. The fitness function for optimisation is therefore defined as $e_1(y) = \|b - Ay\|_2^2$ where Ay is computed, for trials y , by the toolbox.

Discrete TR problems are translatable into real valued problems suitable for optimisers such as PSO and DE by enabling y to take continuous rather than discrete values, $y \in [0, 255]^n$, therefore, allowing e_1 and e_2 to accept real inputs. The original object, x^* , remains discrete. Final solutions y can be discretised for visualisation purposes if necessary.

3 Regularisation

One of the issues associated with image reconstruction is the presence of salt and pepper noise which impacts the fidelity of the reconstructed image to the ground truth. This work uses two approaches to reduce the noise during the reconstruction process: search space expansion (SSE) and total variation regularisation (TV).

3.1 Search space expansion

In SSE, the search space allocated to the optimiser is initially confined to only a portion of the feasible space [7]. Assuming the complete search space to be $\Xi = [0, 255]^n$, the initial space would be defined as $\Xi_1 = [0, \frac{255}{d}]^n$, where $d > 1$. Any particle leaving this initially allocated space is clamped to the edges. The initial search space is then progressively expanded to explore previous unseen territories. Expansions from the initial space to the subsequent expanded ones kick-in at preset intervals during the optimisation. By the end of the optimisation process, the optimiser can access the entire search space.

For empirical trials a series of boxes $\Xi_p = [0, \frac{p}{P} \times 255]^n$ are defined with expansions at equal divisions of the total budget of function evaluations. For example, with five subspaces and a budget of 100,000 function evaluations (FEs), search is conducted in the following boxes:

$$\begin{aligned} \Xi_1 &= [0, \frac{255}{5}]^n, & 0 < FE \leq 20000 \\ \Xi_2 &= [0, \frac{2 \times 255}{5}]^n, & 20000 < FE \leq 40000 \\ \Xi_3 &= [0, \frac{3 \times 255}{5}]^n, & 40000 < FE \leq 60000 \\ \Xi_4 &= [0, \frac{4 \times 255}{5}]^n, & 60000 < FE \leq 80000 \\ \Xi_5 &= [0, 255]^n, & 80000 < FE \leq 100000. \end{aligned}$$

3.2 Total Variation

To perform the reconstruction task, the problem is formulated in order to retrieve the unknown vector y based on the projection matrix A and the observation vector b . In inverse problems such as TR, regularisation attempts to circumvent overfitting [20]. Total Variation (TV) regularisation is a deterministic technique that penalises discontinuities in image processing tasks.

Eq. 2 is augmented with a total variation regularisation term:

$$e_1^{TV}(y) = \|b - Ay\|_2^2 + \mu TV(y) \quad (4)$$

where the first term serves as a data fidelity term, ensuring the consistency between the reconstructed image y and the measurement b , and the second term is the TV semi-norm. $\mu > 0$ controls the influence of the TV term.

The TV norm is

$$TV(y) = \sum_{i,j} \sqrt{|y_{i+1,j} - y_{i,j}|^2 + |y_{i,j+1} - y_{i,j}|^2} \quad (5)$$

where the sum is over 2D pixel locations (i, j) . Regions of small pixel value gradient $|y_{i+1,j} - y_{i,j}|$ and $|y_{i,j+1} - y_{i,j}|$ will minimise $TV(y)$ and provide homogeneous regions of biologically feasible structure. It has been shown that the TV enhancement is robust, and able to remove noise and artefacts in the reconstructed image [37].

4 Minimalist swarm optimiser and TR

Dispersive flies optimisation (DFO) is a slimmed-down particle swarm optimisation (PSO) variant, which is distinguished by the abolition of particle memory. Updates are computed from current, rather than historical, position [2]. The exploration and exploitation behaviour of the algorithm is investigated in [3]. DFO also implements component-wise particle jumps which have been shown to be beneficial in bare bones PSO [15].

The optimisation starts by determining the best overall position g^{t+1} , if unique, and positions of all best ring neighbours in the neighbourhood, n_i^{t+1} of each particle (barring the current swarm best particle, which is not updated). Position component d of all particles i , (other than the swarm best) updates according to

$$\begin{aligned} &\text{if } u \sim U(0, 1) < \Delta \\ &\quad x_{id}^{t+1} \sim U(X_d) \\ &\text{else} \\ &\quad x_{id}^{t+1} = n_{id}^{t+1} + \phi u_1 (g_d^{t+1} - x_{id}^t) \end{aligned} \tag{6}$$

where Δ is a predetermined jump probability and $U(X_d)$ is the uniform distribution along axis d of the search space X , $u_1 \sim U(0, 1)$ and $\phi \in [0, \sqrt{3}]$. The constraint on ϕ is derived from a convergence analysis for stochastic difference equations [15]. The algorithm employs global and local strategies and has two arbitrary parameters N and Δ ; and ϕ is invariably set to 1 in published studies. The algorithm has been applied to a wide range of problems in computer vision, aesthetics measurement and art, optimising food processes, electronics, data science and neuroevolution [8, 1, 11, 33, 9, 10, 4, 14].

5 Experiments and results

The experiments use five phantoms as shown in Fig. 1. Phantoms 1 - 4 are binary images and phantom 5, the Shepp-Logan phantom, is a discrete problem with six pixel value levels [35]. The phantom sizes are 32×32 and 64×64 . To test few-view, undersampled conditions, the number of projections, α , was set to 6, 8, 16 and 32. ASTRA toolbox [43] is used to conduct phantom imaging using parallel geometry with the number of rays set to 32 and 64 for the the 32×32 and 64×64 phantoms respectively.

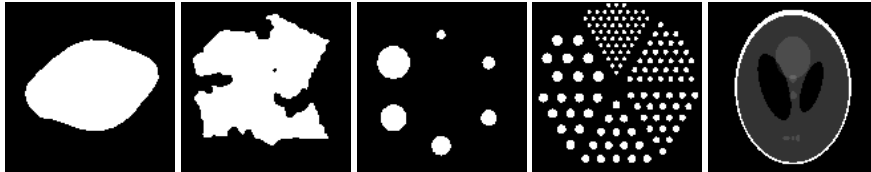


Figure 1: Phantoms

From the ASTRA toolbox, five reference algorithms were selected: filtered backprojection (FBP), the algebraic algorithms ART, SIRT and SART, and a gradient descent reconstruction procedure, CGLS. The potential of swarm reconstruction was tested with three swarm algorithms, PSO (in two varieties, global PSO or GPSO, and local PSO, LPSO), DE and DFO.

The swarm algorithms were run for 100,000 function evaluations. ART, CGLS, FBP, SART and SIRT perform the reconstruction in \mathbb{R}^D , where $D = 32 \times 32$ or 64×64 . Reconstructions were scaled to $X = [0, 255]^D$ for the purpose of computing the reproduction error, e_2 .

A swarm size of $N = 100$ was chosen for G/LPSO, DE and DFO. Particles were initialised in X with the uniform distribution and G/LPSO velocities were set to zero. Particles in all three swarms were clamped to the search box: any particle attempting to leave X was placed on the boundary, and in the case of G/LPSO, velocity is set to zero.

Table 1: Rounded median reconstruction error, e_1 , for each problem and algorithm.

	TR toolbox algorithms					Population-based optimisers			
	ART	CGLS	FBP	SART	SIRT	DE	DFO	GPSO	LPSO
Ph 1 , size = 32^2 , $\alpha = 6$	218	16	57353136	1	0	6213594	6509	36756397	302287
$\alpha = 8$	434	13	55960670	9	0	8972489	0	51413743	33858
$\alpha = 16$	1192	1	12080882	1421	12	15729665	0	104974480	4189
$\alpha = 32$	4767	12	12993996	765224	79	30193881	0	202177910	2387
Size = 64^2 , $\alpha = 6$	511	22	881101300	2	0	449457240	290703650	962231630	128747038
$\alpha = 8$	1993	4	684892900	54	1	612323100	403979650	1338255850	178845160
$\alpha = 16$	5347	8	154832160	977	12	1263333600	777572730	2558892500	343625315
$\alpha = 32$	32556	6	95809730	52562	73	2450199350	1524608650	5098064750	666271775
Ph 2 , size = 32^2 , $\alpha = 6$	682	27	219649500	0	0	4881877	489974	26541697	2598464
$\alpha = 8$	1027	0	125614740	12	0	7757407	290828	36228715	2010975
$\alpha = 16$	1014	4	30864254	1144	12	13824955	0	75870290	163955
$\alpha = 32$	6805	20	34511600	3798144	136	27962292	0	157194035	69490
Size = 64^2 , $\alpha = 6$	21532	25	2552608300	7	0	296865630	205105125	650832450	113333140
$\alpha = 8$	13219	29	1476768100	121	0	385430975	271130845	797472900	157673265
$\alpha = 16$	8634	1	421734660	1859	20	811162880	559093000	1715699050	324069900
$\alpha = 32$	50550	11	278557820	42777	289	1649504250	1108368850	3431840500	634350900
Ph 3 , size = 32^2 , $\alpha = 6$	88	0	118908584	0	0	7825271	134	67812627	736763
$\alpha = 8$	124	0	74234100	1	0	10517076	56	80654290	1326800
$\alpha = 16$	1543	0	9678624	3988	13	24247643	0	168775595	2079945
$\alpha = 32$	5894	2	4692086	4138801	97	42903300	0	330850820	2896024
Size = 64^2 , $\alpha = 6$	3449	0	1572601300	0	0	835896350	503486890	2165751550	195114935
$\alpha = 8$	491	1	1007831400	13	0	1019598350	581618945	2758263850	241910610
$\alpha = 16$	6827	4	188459900	1472	28	2082434150	1198967450	5413350650	515041345
$\alpha = 32$	17844	2	36140108	15064	149	3993287550	2389057650	10727333500	990994525
Ph 4 , size = 32^2 , $\alpha = 6$	217	2	808024770	2	0	4994230	609809	25554527	3385390
$\alpha = 8$	555	1	370298020	30	1	5256030	721491	24894351	4710365
$\alpha = 16$	8929	0	69808620	10431	57	23979954	2613173	72151635	14181106
$\alpha = 32$	47093	2	26453604	4325603	590	60286648	826782	157362800	27365272
Size = 64^2 , $\alpha = 6$	8068	7	13681514000	10	0	261069665	111867240	769442225	85870980
$\alpha = 8$	1008	3	4972211700	1	0	243611335	95635225	714078650	91989665
$\alpha = 16$	12288	0	1202136800	1727	62	582503870	259003385	1622731400	279910750
$\alpha = 32$	78954	1	269898500	240709	702	1278379300	602676550	2860742250	706395100
Ph 5 , size = 32^2 , $\alpha = 6$	322	2	64488092	5	0	3358653	356519	19843914	2682284
$\alpha = 8$	429	0	37028332	102	6	5220447	508443	28824148	4289071
$\alpha = 16$	6785	2	7614852	2373	29	16464641	1470355	66384160	10751817
$\alpha = 32$	5198	2	9878102	90968	74	44725869	4028948	153507290	24552911
Size = 64^2 , $\alpha = 6$	2881	4	1179886800	0	0	240579325	98721218	821075400	69743575
$\alpha = 8$	1581	0	663436700	218	1	328983280	136800775	1059109055	107567910
$\alpha = 16$	5234	0	159528460	890	19	721549070	291544490	2089936600	248175780
$\alpha = 32$	37583	0	62805610	58163	145	1414172750	600360370	4179300750	532845370

Table 2: Algorithms comparison based on e_1 . Numbers indicate statistically significant wins for the algorithm in the left hand column versus the algorithm in the top row.

	ART	CGLS	FBP	SART	SIRT	DE	DFO	GPSO	LPSO	Σ
ART	NA	0	40	12	0	40	31	40	39	202
CGLS	40	NA	40	32	22	40	33	40	40	287
FBP	0	0	NA	0	0	16	9	25	10	60
SART	28	8	40	NA	0	40	32	40	37	225
SIRT	40	18	40	40	NA	40	33	40	40	291
DE	0	0	23	0	0	NA	0	40	0	63
DFO	7	7	31	8	6	40	NA	40	22	161
GPSO	0	0	13	0	0	0	0	NA	0	13
LPSO	1	0	29	3	0	40	18	40	NA	131

Table 3: Rounded median reproduction error, e_2 , for each problem and each algorithm. Lighter shading indicates the proximity of the reconstructions to the phantoms. The largest error in phantoms of sizes 32^2 and 64^2 are 255×32^2 and 255×64^2 respectively.

	TR toolbox algorithms					Population-based optimisers			
	ART	CGLS	FBP	SART	SIRT	DE	DFO	GPSO	LPSO
Ph 1 , size = 32^2 , $\alpha = 6$	51826	99356	82043	52562	52254	13242	420	29844	2773
$\alpha = 8$	51750	66418	86995	52311	53461	11821	1	27672	680
$\alpha = 16$	38745	115808	55146	58775	42220	8124	0	25746	150
$\alpha = 32$	37587	6821	35016	112567	27634	6962	0	24352	80
Size = 64^2 , $\alpha = 6$	216081	217040	425778	214884	246053	159530	142480	220776	97210
$\alpha = 8$	227658	286941	385363	225173	241075	152623	135958	217264	91322
$\alpha = 16$	162459	210787	262494	195464	179756	152407	129482	211900	84812
$\alpha = 32$	132566	130101	181438	464631	150986	149321	128086	210921	80886
Ph 2 , size = 32^2 , $\alpha = 6$	75478	117958	96146	74991	75948	20278	9493	35795	16268
$\alpha = 8$	66315	110549	91503	70612	71292	18407	5107	33860	9631
$\alpha = 16$	53931	104435	67266	62931	52404	11191	0	27210	1327
$\alpha = 32$	35972	16688	45266	119778	29999	8957	0	26880	536
Size = 64^2 , $\alpha = 6$	306143	489520	396555	300664	308809	178848	170864	230096	135870
$\alpha = 8$	271574	457891	408102	275737	280536	173193	164081	227429	129423
$\alpha = 16$	230965	231018	319252	248662	241230	158693	146497	217395	109135
$\alpha = 32$	178735	179516	217124	389843	181413	154848	139559	216685	101305
Ph 3 , size = 32^2 , $\alpha = 6$	54111	110037	75229	53060	61049	11359	34	30476	3542
$\alpha = 8$	69160	77480	87131	70097	65759	12164	19	31467	4563
$\alpha = 16$	43337	77609	57842	87346	40388	10360	0	32132	2537
$\alpha = 32$	33606	9854	36061	110320	31623	8781	0	31635	1756
Size = 64^2 , $\alpha = 6$	239804	376982	396969	236242	243335	164059	138704	238811	90967
$\alpha = 8$	275303	470541	408217	271385	297473	171601	144178	245820	98706
$\alpha = 16$	207820	475237	315308	200323	219470	170917	138741	242887	92402
$\alpha = 32$	141076	142095	192508	482340	141896	169328	138694	246142	89084
Ph 4 , size = 32^2 , $\alpha = 6$	106233	106734	106053	107896	106042	42639	36845	52692	41449
$\alpha = 8$	99030	126284	112713	98011	101802	50782	45347	57539	48984
$\alpha = 16$	78535	109904	93446	118392	90560	38058	22937	50469	32753
$\alpha = 32$	61504	18723	76074	148488	59498	30381	3817	45841	22629
Size = 64^2 , $\alpha = 6$	359476	457919	341521	351830	369252	227959	198832	286299	194556
$\alpha = 8$	370377	508417	397320	379010	402508	242933	216563	288858	216007
$\alpha = 16$	327332	311610	353516	334652	378013	232429	199097	293588	200125
$\alpha = 32$	260130	241566	315026	470472	250627	228127	182692	291675	191472
Ph 5 , size = 32^2 , $\alpha = 6$	81618	125584	85029	82844	80749	42046	37052	53284	41565
$\alpha = 8$	69074	69497	93444	69635	71007	40768	34377	52579	40438
$\alpha = 16$	45410	97915	65674	82172	46194	37515	27831	50481	33405
$\alpha = 32$	25400	1332	45441	91940	15897	34474	21385	47786	29791
Size = 64^2 , $\alpha = 6$	289093	419775	326454	287494	292781	216387	180379	278224	184707
$\alpha = 8$	283383	433439	379237	286974	288103	214797	178452	276883	178909
$\alpha = 16$	225719	230242	291806	253042	224918	214866	171819	279062	170918
$\alpha = 32$	145426	159103	180867	461802	184953	211410	167643	278226	168244

The DFO jump probability was set to 0.001; G/LPSO was run with $w = 0.729844$ and $c = 1.49618$ and the DE/best/1 parameters F and C_R were both set to 0.5. All algorithms with randomisation were run 30 times on each of the 40 problems: 5 phantoms \times 4 projection types (6, 8, 16, 32) \times 2 sizes (32×32 and 64×64).

5.1 Vanilla swarm and toolbox algorithms results

Aggregating the results of Table 1 which summarises the performance of the swarm and toolbox algorithms, Table 2 reports on Wilcoxon statistical significance tests on the reconstruction error for algorithm pairs for the 40 problem instances at a significance level of 0.05. The rows show the number of instances in which the row algorithm performed better than the column algorithm. For example, reading along the first row, ART gave a significantly smaller reconstruction error, e_1 , than SART on 12 of the 40 trials.

Algebraic reconstruction algorithms ART, SART and SIRT and gradient descent, CGLS, uniformly outperform DE, GPSO and LPSO and are better than DFO in at least 31 trials. SIRT presents the best

Table 4: Algorithms comparison based on e_2 . Numbers indicate statistically significant wins for the algorithm in the left hand column versus the algorithm in the top row.

	ART	CGLS	FBP	SART	SIRT	DE	DFO	GPSO	LPSO	Σ
ART	NA	32	37	29	28	4	1	11	2	144
CGLS	8	NA	20	17	13	5	2	12	3	80
FBP	3	20	NA	16	4	1	0	4	0	48
SART	11	23	24	NA	18	0	0	4	0	80
SIRT	12	27	36	22	NA	3	1	10	1	112
DE	36	34	39	40	37	NA	0	40	0	226
DFO	39	38	40	40	39	40	NA	40	22	298
GPSO	28	27	35	35	28	0	0	NA	0	153
LPSO	38	37	40	40	39	39	13	40	NA	286

performance as shown in shaded colour in the last column which sums the total number of significant wins. These results are expected given the toolbox algorithms have been specifically designed for reconstruction while the swarm algorithms are off-the-shelf multi-purpose low-dimensional optimisers that have not been tuned to the reconstruction task.

In Table 4, comparing algorithm pairs based on the reproduction error, e_2 , illustrates that DE, LPSO (and to a lesser extent GPSO) consistently find better reproductions than any of the toolbox algorithms; and DFO produces better results than the rest of the swarm and toolbox algorithms.

Table 3 presents the median reproduction error of each algorithm over each set of problem. Lighter shading indicates lower e_2 error. DFO generates good reproduction, followed by LPSO. DFO produces exact reconstruction of the original phantoms ($e_2 = 0$) in 6 out of 40 experiments, where no other swarm or toolbox algorithm is capable of producing an exact reconstruction.

5.2 Parameter tuning

To better optimise the leading swarm method in the context of the problem, DFO parameters were fine-tuned. Phantom 1, with size 32×32 and $\alpha = 6$, was used as a benchmark to sweep through the parameter space. The parameters tuned are N , ϕ and Δ , and DFO was used as a hyper-parameter optimiser. The optimiser was run 30 times with the population size of 10 and the termination criterion set to 100 iterations (1000 function evaluations). During the fine-tuning exercise, the elitism mechanism was revised, catering for the presence of stochasticity in the optimisation process, and to enable re-evaluation of the current best particle parameters found in the trials. The optimum and most frequent successful parameter values found were $\Delta = 0.001$, $N = 2$ and $\phi = 1.7320508 \approx \sqrt{3}$. The small value of optimal N confirms the finding that the function profile has a single broad funnel leading the global optima, in effect rendering the task into a largely unimodal problem [6]. It also indicates that DFO is acting as a ‘swarm-inspired local search’ and the collective presence of a large communication network is unnecessary in this context. Three local search algorithms (Nelder-Mead [31], L-BFGS-B [46], MTS-LS1 [41]), had been investigated, demonstrating that a ‘simple’ local search may fall short of competing with ‘a swarm-based local search’.

5.3 Search space expansion

The positive impact of SSE has been studied by researchers. In this work, first SSE is fine-tuned on Shepp-Logan phantom, which was introduced in 1974, and is a schematic representation of a cranial slice [35] (a standard phantom for TR algorithm testing); then, the fitness function is adapted to integrate the TV regularisation term (Eq. 4). Fine-tuning SSE identifies the optimal number of expanding boxes required to reduce the noise in the reconstructed images.

As a result, Table 5 presents the median errors for the reconstruction and reproduction errors, e_1 and e_2 respectively, for 30 runs.

While a single box produces the smallest median reconstruction error (see the first row in Table 5, and Table 6-left), the result is distant from the original phantom (see the corresponding e_2 error and Fig. 2); 50 boxes, however, produces a better reproduction error, with the reconstructed image closer

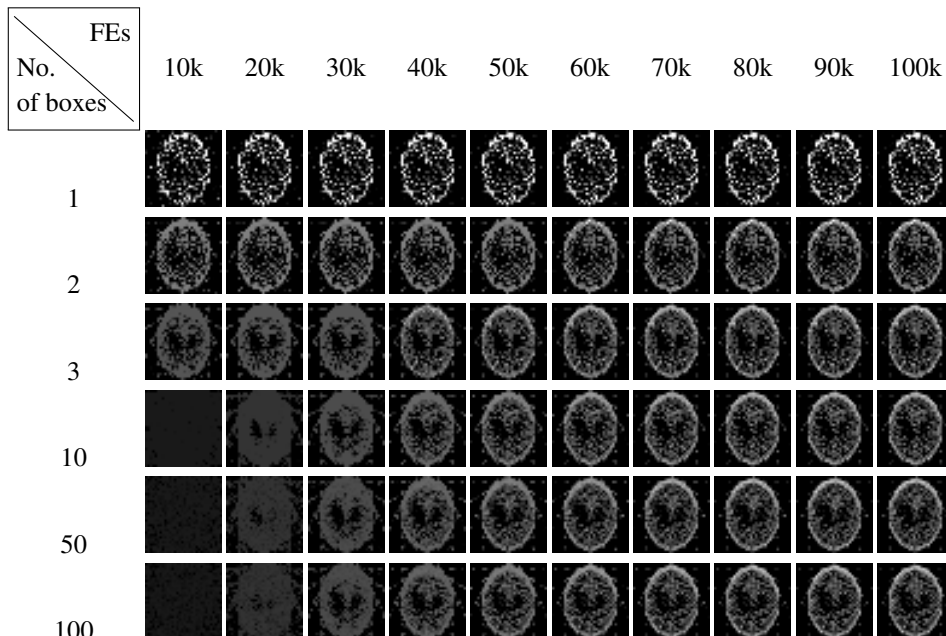


Figure 2: Visualising the reconstruction process of Shepp-Logan phantom at different points in the optimisation process (every 10,000 FEs) and for varying number of expanding boxes, with phantom size of 32×32 and 6 projections.

Table 5: Median error values for 30 runs on each of five boxing scenarios for 32×32 Shepp-Logan, imaged with 6 projections. The smallest e_1 and e_2 errors are highlighted.

Boxes	e_1	e_2
1	47222	32642
2	113234	24731
3	102552	20463
10	110200	20085
50	114391	19662
100	120111	19957

to the original. Increasing the number of boxes beyond 50 does not statistically significantly alter the e_2 outcome (see last row in Table 6-right).

5.4 Total variation regularisation

Total variation regularisation is another tool in ‘denoising’ images during the reconstruction process. The successful use of this method depends highly on adjusting the μ parameter (Eq. 4). To conduct the fine-tuning, a range of values from $\mu = [0, 1000]$ are selected and 30 independent trials are run for each μ value. Table 7 presents (a) the median error values for both e_1 and e_2 , along with (b) the statistical analysis of the results. Based on the statistical analysis of the reproduction error, the ‘sweet spot’ for the regularisation parameter is between $\mu = [40, 65]$, with the best value $\mu = 55$ with 19 significant wins out of 25. The regularisation, which is studied here, follows the search space expansion, and serves the similar purpose of smoothing the reconstructed images by balancing the trade off between a smaller e_1 error with a more clinically plausible reconstruction. We notice that, as in the boxing scenarios, regularisation degrades the e_1 error as shown in Table 7 (the best e_1 is obtained when $\mu = 0$), but improves the overall reconstruction, as seen from its impact on e_2 error.

Table 6: Statistical analysis of e_1 (left) and e_2 (right) for varying boxing scenarios for 32×32 Shepp Logan with 6 projections. A ‘1’ indicates a Wilcoxon win for the algorithm over 30 runs in the left hand column versus the algorithm in the top row. ‘0’ indicates no significant difference in the algorithms. For the reproduction error, there are no significant differences from boxing scenario 50.

e_1							e_2						
Boxes	1	2	3	10	50	100	Boxes	1	2	3	10	50	100
1	NA	1	1	1	1	1	1	NA	0	0	0	0	0
2	0	NA	0	0	0	1	2	1	NA	0	0	0	0
3	0	1	NA	1	1	1	3	1	1	NA	0	0	0
10	0	0	0	NA	1	1	10	1	1	1	NA	0	0
50	0	0	0	0	NA	1	50	1	1	1	1	NA	0
100	0	0	0	0	0	NA	100	1	1	1	1	0	NA

Table 7: Total variation regularisation. (a) e_1 and e_2 median error values for varying μ , along with (b) the count of statistically significant wins for each μ .

μ	(a) Error values		(b) Statistically significant cases	
	e_1	e_2	e_1	e_2
0	118549	19833	24	1
1	176868	19457	23	2
5	401477	18274	22	3
10	642329	17213	21	4
15	846614	16379	20	6
20	1033289	15807	19	8
25	1216424	15353	18	9
30	1386386	14972	17	12
35	1556795	14734	16	16
40	1719532	14580	15	18
45	1889283	14630	14	17
50	2052300	14625	13	18
55	2187202	14650	12	19
60	2352773	14672	11	16
65	2507530	14577	10	18
70	2665960	14762	9	15
75	2813415	14682	8	14
80	2957201	14861	7	13
85	3098517	14906	6	13
90	3249197	15097	5	12
95	3410860	15243	4	9
100	3539566	15306	3	9
150	4899699	16182	2	6
200	6174531	17193	1	4
1000	24795852	25632	0	0

5.5 Comparison with SHADE-ILS algorithm

The standard version of the optimisers used in this work are designed for lower dimensional problems. Large-scale global optimisation (LSGO), which deals with a great number of variables, has been gaining increasing popularity in recent years. One such method, SHADE with iterative local search or SHADE-ILS [30], which has won the CEC’2018 LSGO competition, hybridises SHADE and two local search methods: MTS-L1 [42] and L-BFGS-B [47]. The performance of this algorithm along with its use of local search methods, provides a good basis for comparison with the proposed swarm technique. In this comparison, the optimised DFO for TR, with neither the search space expansion nor total variation regularisation (DFO-TR), is compared against DFO-TR with search space expansion and total variation regularisation (DFO-TR- μ), the best performing TR toolbox algorithm (SIRT), and SHADE-ILS.

Wilcoxon significance results for 30 runs on Shepp-Logan phantom are given in Table 8. Table 8-left compares algorithm pairs when rated according to the reconstruction error, e_1 . Unsurprisingly, SIRT produces the best reconstruction, e_1 (followed by SHADE-ILS); while DFO-TR does not offer a statistically significant difference with SHADE-ILS in image reproduction, e_2 , DFO-TR- μ which

Table 8: Comparison with SHADE-ILS. A ‘1’ indicates a Wilcoxon win for the algorithm over 30 runs in the left hand column versus the algorithm in the top row. ‘0’ indicates no significant difference in the algorithms.

e_1	DFO-TR	DFO-TR- μ	SIRT	SHADE-ILS
DFO-TR	NA	1	0	0
DFO-TR- μ	0	NA	0	0
SIRT	1	1	NA	1
SHADE-ILS	1	1	0	NA

e_2	DFO-TR	DFO-TR- μ	SIRT	SHADE-ILS
DFO-TR	NA	0	1	0
DFO-TR- μ	1	NA	1	1
SIRT	0	0	NA	0
SHADE-ILS	0	0	1	NA

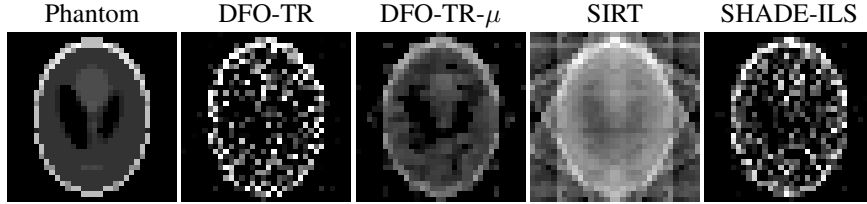


Figure 3: Reconstructing Shepp-Logan by the swarm optimiser without the smoothing methods (DFO-TR), the presented method with dual regularisation of search space expansion and the total variation (DFO-TR- μ), the best standard TR toolbox algorithm (SIRT), and SHADE-ILS.

benefits from the dual regularisation methods, produces statistically significant smaller reproduction errors (Table 8-right).

Fig. 3 shows the visual reconstruction of the Shepp-Logan phantom using the four aforementioned techniques. The figure shows the presence of artefacts in SIRT, and salt-and-pepper noise in both DFO-TR and SHADE-ILS. Under this highly undersampled scenario, DFO-TR- μ presents a respectable reconstruction of the phantom, albeit with yet some distance from a zero reproduction error.

6 Conclusion

This work investigates two regularisation methods in the context of tomographic reconstruction when dealing with highly undersampled data in few-view scenarios. These methods – search space expansion and total variation – are sequentially fine-tuned and adapted to the reconstructing algorithm. Integrating these methods results in the worsening of the reconstruction errors, which was expected; however, the presented pipeline, and the use of the updated objective function, result in lower reproduction errors, which demonstrates a more faithful reconstruction to the ground truth than the standard toolbox algorithms and a high-dimensional optimiser. Among the subjects of future research is reformulating the problem into a multiobjective problem as well as hybridising classical toolbox techniques (with their signature feature of low reconstruction error) and the presented swarm optimisation method, benefiting from dual regularisation (with low reproduction errors) which could produce a powerful algorithm capable of fast noise- and artefacts-free reconstructions in the few-view regime.

References

- [1] Bishwa Babu Acharya, Sandeep Dhakal, Aayush Bhattarai, and Nawraj Bhattarai. Pid speed control of dc motor using meta-heuristic algorithms. *International Journal of Power Electronics and Drive Systems*, 12(2):822, 2021.
- [2] Mohammad Majid al-Rifaie. Dispersive flies optimisation. In *2014 Federated Conference on Computer Science and Information Systems*, pages 529–538. IEEE, 2014.
- [3] Mohammad Majid al-Rifaie. Exploration and exploitation zones in a minimalist swarm optimiser. *Entropy*, 23(8):977, 2021.

- [4] Mohammad Majid al-Rifaie and Ahmed Aber. Dispersive flies optimisation and medical imaging. In *Recent Advances in Computational Optimization*, pages 183–203. Springer, 2016.
- [5] Mohammad Majid al-Rifaie and Tim Blackwell. *Applications of Evolutionary Computation: 19th European Conference, EvoApplications 2016, Porto, Portugal, March 30 – April 1, 2016, Proceedings, Part I*, chapter Binary Tomography Reconstruction by Particle Aggregation, pages 754–769. Springer International Publishing, Cham, 2016.
- [6] Mohammad Majid al-Rifaie and Tim Blackwell. Swarm led tomographic reconstruction. In *Proceedings of the Genetic and Evolutionary Computation Conference, GECCO '22*, page 1121–1129, New York, NY, USA, 2022. Association for Computing Machinery.
- [7] Mohammad Majid al-Rifaie and Tim Blackwell. Tomographic reconstruction with search space expansion. In *Proceedings of the Genetic and Evolutionary Computation Conference*, pages 1286–1293, 2023.
- [8] Mohammad Majid al-Rifaie and Marc Cavazza. Evolutionary optimisation of beer organoleptic properties: A simulation framework. *Foods*, 11(3):351, Jan 2022.
- [9] Mohammad Majid al-Rifaie, Anna Ursyn, Robert Zimmer, and Mohammad Ali Javaheri Javid. On symmetry, aesthetics and quantifying symmetrical complexity. In João Correia, Vic Ciesielski, and Antonios Liapis, editors, *Computational Intelligence in Music, Sound, Art and Design: EvoMUSART 2017*, pages 17–32. Springer International Publishing, 2017.
- [10] Haya Abdullah Alhakbani and Mohammad Majid al-Rifaie. Optimising svm to classify imbalanced data using dispersive flies optimisation. In *2017 Federated Conference on Computer Science and Information Systems (FedCSIS)*, pages 399–402. IEEE, 2017.
- [11] Prashant Aparajeya, Frederic Fol Leymarie, and Mohammad Majid al-Rifaie. Swarm-based identification of animation key points from 2d-medialness maps. In Anikó Ekárt, Antonios Liapis, and María Luz Castro Pena, editors, *Computational Intelligence in Music, Sound, Art and Design*, pages 69–83, Cham, 2019. Springer International Publishing.
- [12] Kees Joost Batenburg and Walter A Kusters. Solving Nonograms by combining relaxations. *Pattern Recognition*, 42(8):1672–1683, 2009.
- [13] Kees Joost Batenburg and Willem Jan Palenstijn. On the reconstruction of crystals through discrete tomography. In *International Workshop on Combinatorial Image Analysis*, pages 23–37. Springer, 2004.
- [14] J. Mark Bishop and Mohammad Majid al-Rifaie. Autopoiesis in creativity and art. In *Proceedings of the 3rd International Symposium on Movement and Computing, MOCO '16*, pages 27:1–27:6, New York, NY, USA, 2016. ACM.
- [15] Tim Blackwell. A study of collapse in bare bones particle swarm optimization. *IEEE Transactions on Evolutionary Computation*, 16(3):354–372, 2011.
- [16] MD Butala, RJ Hewett, RA Frazin, and F Kamalabadi. Dynamic three-dimensional tomography of the solar corona. *Solar Physics*, 262(2):495–509, 2010.
- [17] Emmanuel J Candes, Justin K Romberg, and Terence Tao. Stable signal recovery from incomplete and inaccurate measurements. *Communications on pure and applied mathematics*, 59(8):1207–1223, 2006.
- [18] José-Maria Carazo, CO Sorzano, Eicke Rietzel, R Schröder, and Roberto Marabini. Discrete tomography in electron microscopy. In *Discrete Tomography*, pages 405–416. Springer, 1999.
- [19] Bruno Carvalho, Gabor Herman, Samuel Matej, Claudia Salzberg, and Eilat Vardi. Binary tomography for triplane cardiography. In *Information Processing in Medical Imaging*, pages 29–41. Springer, 1999.
- [20] Antonin Chambolle. An algorithm for total variation minimization and applications. *Journal of Mathematical imaging and vision*, 20:89–97, 2004.
- [21] Marco Cipolla, Giosuè Lo Bosco, Filippo Millonzi, and Cesare Valenti. An island strategy for memetic discrete tomography reconstruction. *Information Sciences*, 257:357–368, 2014.
- [22] Richard J Gardner. *Geometric tomography*, volume 1. Cambridge University Press Cambridge, 1995.

- [23] Lucas L Geyer, U Joseph Schoepf, Felix G Meinel, John W Nance Jr, Gorka Bastarrika, Jonathon A Leipsic, Narinder S Paul, Marco Rengo, Andrea Laghi, and Carlo N De Cecco. State of the art: iterative ct reconstruction techniques. *Radiology*, 276(2):339–357, 2015.
- [24] A. Giussani and C. Hoeschen. *Imaging in nuclear medicine*. Springer, 2013.
- [25] U Hampel, A Bieberle, D Hoppe, J Kronenberg, E Schleicher, T Sühnel, F Zimmermann, and C Zippe. High resolution gamma ray tomography scanner for flow measurement and non-destructive testing applications. *Review of scientific instruments*, 78(10):103704, 2007.
- [26] Gang Hu, Min-you Chen, Wei He, and Jin-qian Zhai. Clustering-based particle swarm optimization for electrical impedance imaging. *Advances in Swarm Intelligence*, pages 165–171, 2011.
- [27] R.W. Irving and M.R. Jerrum. Three-dimensional data security problems. *SIAM J. Comput.*, 23:170–184, 1994.
- [28] Fethi Jarray and Ghassen Tlig. A simulated annealing for reconstructing hv-convex binary matrices. *Electronic Notes in Discrete Mathematics*, 36:447–454, 2010.
- [29] Póth Miklós. Particle swarm optimization approach to discrete tomography reconstruction problems of binary matrices. In *Intelligent Systems and Informatics (SISY), 2014 IEEE 12th International Symposium on*, pages 321–324. IEEE, 2014.
- [30] Daniel Molina, Antonio LaTorre, and Francisco Herrera. Shade with iterative local search for large-scale global optimization. In *2018 IEEE congress on evolutionary computation (CEC)*, pages 1–8. IEEE, 2018.
- [31] John A Nelder and Roger Mead. A simplex method for function minimization. *The computer journal*, 7(4):308–313, 1965.
- [32] Guust Nolet et al. A breviary of seismic tomography. *Imaging the Interior*, 2008.
- [33] Hooman Oroojeni, Mohammad Majid al-Rifaie, and Mihalis A. Nicolaou. Deep neuroevolution: Training deep neural networks for false alarm detection in intensive care units. In *European Association for Signal Processing (EUSIPCO) 2018*, pages 1157–1161. IEEE, 2018.
- [34] Ahlem Ouaddah and Dalila Boughaci. Improving reconstructed images using hybridization between local search and harmony search meta-heuristics. In *Proceedings of the Companion Publication of the 2014 Annual Conference on Genetic and Evolutionary Computation*, pages 1475–1476. ACM, 2014.
- [35] Lawrence A Shepp and Benjamin F Logan. The fourier reconstruction of a head section. *IEEE Transactions on nuclear science*, 21(3):21–43, 1974.
- [36] Abe R. Shliferstein and YT Chien. Some properties of image-processing operations on projection sets obtained from digital pictures. *IEEE Transactions on Computers*, 26(10):958–970, 1977.
- [37] Emil Y Sidky and Xiaochuan Pan. Image reconstruction in circular cone-beam computed tomography by constrained, total-variation minimization. *Physics in Medicine & Biology*, 53(17):4777, 2008.
- [38] Zhen Tian, Xun Jia, Kehong Yuan, Tinsu Pan, and Steve B Jiang. Low-dose ct reconstruction via edge-preserving total variation regularization. *Physics in Medicine & Biology*, 56(18):5949, 2011.
- [39] Ana Carolina Trevisan, Michel David Raed, Vitor Tumas, Leonardo Alexandre-Santos, Felipe Arriva Pitella, Emerson Nobuyuki Itikawa, Jose Henrique Silvah, Mery Kato, Edson Zangiomi Martinez, Jorge Alberto Achcar, et al. Comparison between osem and fbp reconstruction algorithms for the qualitative and quantitative interpretation of brain dat-spect using an anthropomorphic striatal phantom: implications for the practice. *Research on Biomedical Engineering*, 36(1):77–88, 2020.
- [40] Jens Tronicke, Hendrik Paasche, and Urs Böniger. Crosshole traveltime tomography using particle swarm optimization: A near-surface field example. *Geophysics*, 77(1):R19–R32, 2012.
- [41] Lin-Yu Tseng and Chun Chen. Multiple trajectory search for large scale global optimization. In *2008 IEEE Congress on Evolutionary Computation (IEEE World Congress on Computational Intelligence)*, pages 3052–3059. IEEE, 2008.

- [42] Lin-Yu Tseng and Chun Chen. Multiple trajectory search for large scale global optimization. In *2008 IEEE congress on evolutionary computation (IEEE world congress on computational intelligence)*, pages 3052–3059. IEEE, 2008.
- [43] Wim Van Aarle, Willem Jan Palenstijn, Jeroen Cant, Eline Janssens, Folkert Bleichrodt, Andrei Dabravolski, Jan De Beenhouwer, K Joost Batenburg, and Jan Sijbers. Fast and flexible x-ray tomography using the astra toolbox. *Optics express*, 24(22):25129–25147, 2016.
- [44] Floris HP van Velden, Reina W Kloet, Bart NM van Berckel, Saskia PA Wolfensberger, Adriaan A Lammertsma, and Ronald Boellaard. Comparison of 3d-op-osem and 3d-fbp reconstruction algorithms for high-resolution research tomograph studies: effects of randoms estimation methods. *Physics in Medicine & Biology*, 53(12):3217, 2008.
- [45] P Wang, JS Lin, and M Wang. An image reconstruction algorithm for electrical capacitance tomography based on simulated annealing particle swarm optimization. *Journal of applied research and technology*, 13(2):197–204, 2015.
- [46] Ciyou Zhu, Richard H Byrd, Peihuang Lu, and Jorge Nocedal. Algorithm 778: L-bfgs-b: Fortran subroutines for large-scale bound-constrained optimization. *ACM Transactions on mathematical software (TOMS)*, 23(4):550–560, 1997.
- [47] Ciyou Zhu, Richard H Byrd, Peihuang Lu, and Jorge Nocedal. Algorithm 778: L-bfgs-b: Fortran subroutines for large-scale bound-constrained optimization. *ACM Transactions on mathematical software (TOMS)*, 23(4):550–560, 1997.